Chinese Chemical Letters 36 (2025) 110511

Contents lists available at ScienceDirect

Chinese Chemical Letters

journal homepage: www.elsevier.com/locate/cclet

Efficient solution-processed near-infrared organic light-emitting diodes with a binary-mixed electron transport layer

Haowen Shang[a], Yujie Yang[b], Bingjie Xue[b], Yikai Wang[b], Zhiyi Su[b], Wenlong Liu[b], Youzhi Wu[a,*], Xinjun Xu[b,*]

[a] School of Materials Science and Engineering, Lanzhou University of Technology, Lanzhou 730050, China
[b] Key Laboratory of Energy Conversion and Storage Materials, College of Chemistry, Beijing Normal University, Beijing 100875, China

ARTICLE INFO

Article history:
Received 3 June 2024
Revised 24 September 2024
Accepted 26 September 2024
Available online 27 September 2024

Keywords:
Near-infrared electroluminescence
Organic light-emitting diodes
Electron transport layer
Nonfullerene acceptor
Solution-processing

ABSTRACT

A binary-mixed electron transport layer (ETL) has been reported for constructing solution-processable near-infrared organic light-emitting diodes (NIR OLEDs). Relative to the single-component ETL, the binary-mixed ETL composed of PDINN:TPBi can enhance the carrier transport capacity, reduce device impedance, and weaken fluorescence quenching of the emitting layer. By carefully selecting an appropriate luminescent material Y5 (a nonfullerene electron acceptor in organic solar cells) and precisely fine-tuning the molecular aggregation in active layer using a mixed solvent, the morphology is optimized and luminescence performance is enhanced, resulting in efficient NIR OLEDs with an emission peak at 890 nm. The experiment showcases a Y5-based near-infrared OLED with a maximum radiance of 34.9 W sr^{-1} m^{-2} and a maximum external quantum efficiency of 0.50%, which is among the highest values reported for non-doped fluorescent NIR OLEDs with an emission peak over 850 nm.

The near-infrared (NIR) region refers to the wavelength range of 700–2500 nm. Organic light-emitting diodes (OLEDs) operating within this band find extensive applications in night vision, biological imaging, photodynamic therapy, agriculture, telecommunications, security authentication, and other fields [1-5]. Specifically, light in the NIR-I region (700–1000 nm), which can effectively penetrate biological tissues, is widely employed in medical fields such as biological imaging and photothermal therapy due to its significant role as a crucial window for light transmission. It is noteworthy that pure organic fluorescent emitters are devoid of heavy metals, rendering them highly biocompatible and environmentally friendly, thus positioning them as the preferred choice for these applications [6-10].

However, practical application of OLEDs in the NIR range is currently unfeasible. Firstly, the emission peak wavelength λ_{EL} is short, primarily due to limitations imposed by the energy gap law [11-17]. This law predicts that non-radiative decay rates in organic solids exponentially increase as the energy gap decreases, resulted from enhanced coupling between electrons and phonons between excited and ground states. Consequently, this limitation implies that long-wave emission from organic solids would be significantly weakened, thereby presenting a major technical bottleneck for extending emissions towards longer wavelengths. Secondly, the enhancement of luminous efficiency in near-infrared luminescent materials poses a significant challenge, thereby impeding their application in OLEDs and hindering their overall development. Doping is a method to enhance the luminous efficiency, as it can regulate the energy levels and mobilities of carriers in materials, together with suppressing concentration induced fluorescence quenching. Up to now, researchers have proposed various doping strategies, however, several inherent problems exist within these doping devices. (1) The selection of appropriate host materials for different colors of dopants is crucial. (2) Controlling the co-deposition rate and concentration of dopants during preparation processes, particularly for low doping concentrations ranging from 0.1% to 1%, remains a challenging task. (3) Careful consideration should be given to the influence of host material carrier mobilities and energy levels on other functionalities within the doped luminescent system. (4) Simultaneous utilization of both a host material and a dopant inevitably leads to increased costs. To avoid these drawbacks, in this study, we will fabricate NIR-OLED devices employing non-doped pure organic materials.

Compared to vacuum evaporation, the solution method offers device fabrication with simpler and more economical equipment, thereby reducing preparation costs. Furthermore, the solution method enables precise control over device structure and performance through parameter adjustments such as solution concen-

* Corresponding authors.
E-mail addresses: youzhiwu@163.com (Y. Wu), xuxj@bnu.edu.cn (X. Xu).

https://doi.org/10.1016/j.cclet.2024.110511
1001-8417/

tration, coating technology, and heat treatment conditions. However, the challenges of solvent and material solubility issues, where previously deposited films may partially or completely dissolve, remain a major obstacle to constructing solution-processed multilayer OLED devices [18-26]. At present, most reports on OLEDs prepared by solution method only have the light-emitting layer undergone solution processing. However, other necessary functional layers, especially electron transport layer (ETL), still need to be prepared by vacuum evaporation [27-31]. Although some studies have proposed the method of realizing all-solution method for multilayer OLEDs using specific orthogonal solvent strategies and a small amount of cross-linked functional materials, this method still has limitations due to factors such as the similar polarity of most organic molecules and the low selectivity of suitable cross-linked materials. In addition, there are still limitations in terms of carrier (electron) injection and transport, so it is necessary to develop a high-performance, solution-processable ETL [32-34].

In recent years, the development of organic solar cells has entered a new era characterized by highly efficient charge separation and low voltage loss, attributed to the emergence of a novel class of nonfullerene electron acceptors with an acceptor-donor-acceptor (A-D-A) molecular structure. This advancement is primarily driven by the strong intramolecular charge transfer effects and rigid planar configurations exhibited by these A-D-A type organic semiconductors, which enhance π-electron delocalization, resulting in reduced band gap and increased oscillation intensity for enhanced near-infrared absorption coefficient. Moreover, A-D-A type organic semiconductors offer several additional advantageous features crucial for minimizing energy loss in organic solar cells including sharp optical absorption edges, suppressed non-radiative recombination rates, low energy disorder, and high luminescence (radiative recombination) yields. Considering the reciprocity between light absorption and emission, these properties render this unique organic semiconductor not only an optimal choice for solar cells but also offer novel insights into constructing high-efficiency non-doped organic fluorescent NIR-OLEDs. Nonfullerene electron acceptor compounds (such as Y5) have high external electroluminescence quantum efficiency values in organic solar cells, and their electroluminescence (EL) emission wavelength can locate over 800 nm. Additionally, such molecules form J aggregates through end-to-end overlap stacking in the solid state, making them a potential near-infrared organic electroluminescent material. Consequently, here we fabricate non-doped NIR-OLED devices employing such nonfullerene acceptor materials.

In addition, in this study, a novel method was employed to treat the ETL to optimize the performance of solution-treated non-doped NIR-OLED. Specifically, two different electron transport materials were dissolved in the same solvent (methanol) and physically blended to prepare a binary-mixed electron transport layer. The two electron transport materials are *N*,*N*′-bis[3-[3(dimethylamino)propylamino]propyl]-perylene-3,4:9,10-bis(dicarboximide) (PDINN) and 1,3,5-tris(1-phenyl-1*H*-benzimidazol-2-yl)benzene (TPBi). PDINN is commonly employed as a cathode modification layer in organic solar cells due to its high solubility in alcohol solvents, which facilitates convenient solution processing. Moreover, PDINN can effectively decrease the work function of the air-stabilized cathode (silver and copper) while maintaining optimal interface contact with the active layer. Currently, the use of PDINN as an ETL in OLED devices has not been reported. TPBi is widely used as an ETL in OLED devices, effectively mitigating the exciton-hole interaction-induced hole quenching effect and thereby significantly enhancing the overall efficiency. However, TPBi is commonly employed as an evaporated ETL, and its application in solution-processed NIR-OLEDs remains unexplored. Our results demonstrate a significant enhancement in electron mobility for the binary-mixed ETL compared to that of the single-component ETL device. The impedance spectroscopy tests demonstrate a decrease in the resistance of the binary-mixed ETL, leading to an enhancement in conductivity. Therefore, the incorporation of PDINN blended with TPBi at a ratio of 1:4 significantly enhances the external quantum efficiency (EQE) for 2,2′-((2*Z*,2′*Z*)-((12,13-bis(2-ethylhexyl)-3,9-diundecyl-12,13-dihydro-[1,2,5]thiadiazolo[3,4-*e*]thieno[2″,3″:4′,5′]thieno[2′,3′:4,5]pyrrolo[3,2-*g*]thieno[2′,3′:4,5]-thieno[3,2-*b*]indole-2,10-diyl)bis(methanylylidene))bis(3-oxo-2,3-dihydro-1*H*-indene-2,1-diylidene))dimalononitrile (Y5)-based NIR OLEDs ($\lambda_{EL} = 890$ nm), resulting in an EQE improvement from 0.41% and 0.45% to 0.50%, which is among the highest efficiency for non-doped fluorescent NIR-OLED [35].

To evaluate the effect of the binary-mixed ETL on the device performance, OLEDs are fabricated using a device structure of indium tin oxide (ITO)/[2-(9*H*-carbazol-9-yl)ethyl]phosphonic acid (2PACz)/emissive layer (EML) (100 nm)/PDINN:TPBi (10 nm)/Ag (100 nm). The molecular structures of EML and ETL components are illustrated in Fig. 1a. Their UV absorption and the photoluminescence (PL, for Y5) spectra are shown in Fig. 1b. We observed strong absorptions in the film states of TPBi and PDINN within the wavelength ranges of 310–350 nm and 420–520 nm, respectively. Additionally, Y5 exhibited significant absorption in the film state at wavelengths ranging from 600 nm to 780 nm [36], and its fluorescence emission peak locates at 940 nm. Therefore, it is a suitable material as an emissive layer in near-infrared OLEDs.

We adopted a method of introducing poor solvent to treat the EML. Briefly, a mixed solvent was prepared by adding 0.5% (v/v) acetonitrile (ACN) to chloroform (CF), which was used to regulate the aggregation behavior of light-emitting material Y5. To gain a more precise comprehension of the morphological changes in the EML deposited from mixed solvent, we primarily investigated the molecular stacking characteristics of Y5 thin films with varying blending ratios using 2-dimensional (2D) grazing-incidence wide-angle X-ray scattering (GIWAXS), as shown in Fig. 2. From Figs. 2a and b, it is evident that the lamellar stacking corresponds to diffraction peaks in the q_{xy} range of 0–0.5 $Å^{-1}$ undergoes a transition from ordered to disordered morphology upon the introduction of ACN (0.5% case). However, within the q_z range of 1.5–2 $Å^{-1}$, diffraction peaks representing π-π stacking of molecules remain discernible. Nevertheless, Figs. 2c and d demonstrate that a further increase in ACN concentration (1% and 5% cases) leads to almost complete disappearance of ordered π-π stacking among small molecules. This indicates that by introducing an appropriate amount of ACN as a mixed solvent, the EML retains a certain level of organization in micro-scale regions while transitioning to disorder on a macro-scale. Ultimately, with increasing the ACN content, disorder further intensifies and crystalline peaks vanish (*i.e.*, even the microscopic order is also disrupted). Therefore, in the CF + 0.5% ACN case, the retained microscopic order facilitates charge transport and exciton delocalization, which is beneficial to enhance radiation decay [37]; meanwhile, the disordered lamellar stacking can prevent exciton from diffusing to the low-energy traps. As a result, the EQE and radiance in the corresponding devices are improved. In contrast, the introduction of excessed ACN (1% and 5%) in the solvent will make Y5 molecules completely disordered, thus being disadvantageous to charge transport and exciton delocalization. For detailed device information, please refer to the Supplementary materials (Fig. S1 and Table S1 in Supporting information).

In order to analyze the effect of different processing solvents on the electro-optical properties of emissive layers, we characterized charge transport in devices. The electron and hole mobilities of the active layer were measured *via* electron-only devices with an ITO/ZnO/Y5/PDINN/Ag structure and hole-only devices with an ITO/2PACz/Y5/MnO_3/Ag structure using the space-charge-limited current (SCLC) method [38,39], as shown in Fig. S2

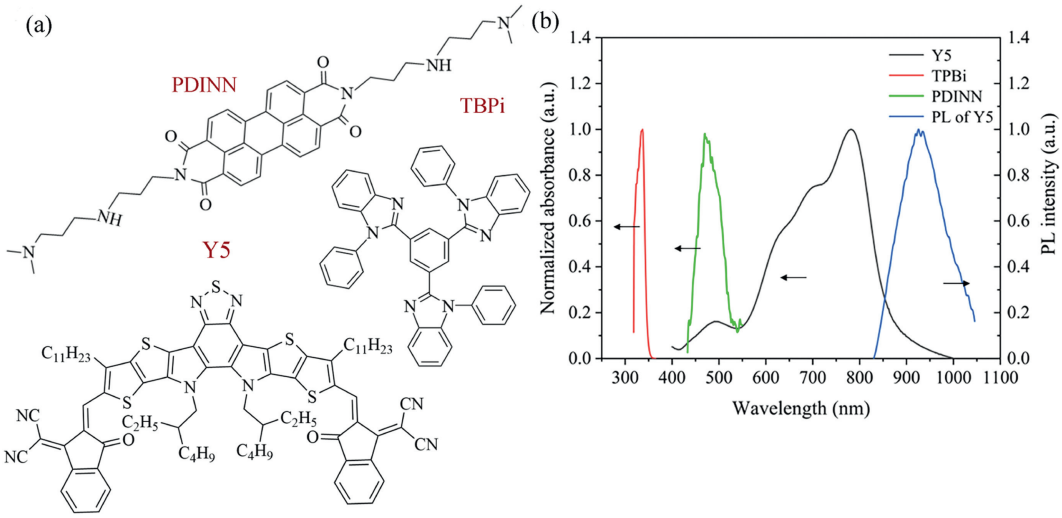

Fig. 1. (a) Molecular structures and (b) UV absorption and PL emission spectra of the main components.

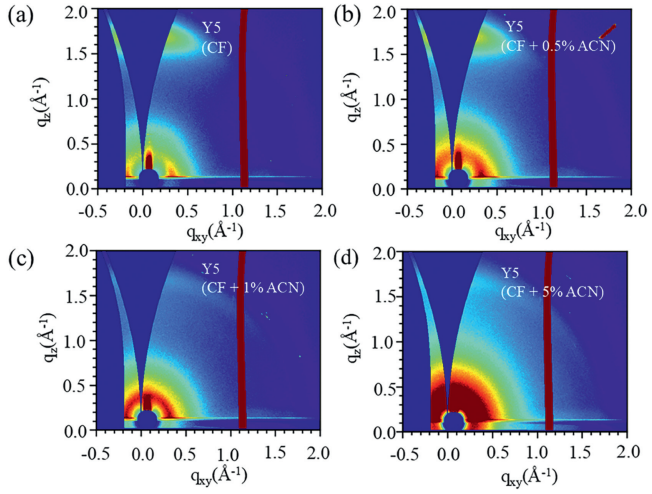

Fig. 2. 2D GIWAXS patterns of Y5 films deposited from different solvents: (a) CF, (b) CF + 0.5% ACN, (c) CF + 1% ACN, and (d) CF + 5% ACN.

Table 1
Electron and hole mobilities of Y5 in devices deposited from different solvents.

Solvent	μ_e ($cm^2\ V^{-1}\ s^{-1}$)	μ_h ($cm^2\ V^{-1}\ s^{-1}$)	μ_e/μ_h
CF	6.96×10^{-4}	3.02×10^{-4}	2.30
CF + 0.5% ACN	7.25×10^{-4}	5.37×10^{-4}	1.35

(Supporting information). The results of calculated mobilities are summarized in Table 1. After using the mixed solvent (CF + 0.5% ACN), the electron mobility increases from 6.96×10^{-4} $cm^2\ V^{-1}\ s^{-1}$ to 7.25×10^{-4} $cm^2\ V^{-1}\ s^{-1}$, and the hole mobility increases from 3.02×10^{-4} $cm^2\ V^{-1}\ s^{-1}$ to 5.37×10^{-4} $cm^2\ V^{-1}\ s^{-1}$. The closer hole and electron mobility values manifest that the charge transport in OLEDs becomes more balanced, thus are beneficial to the improvement in electroluminescence (EL) performance.

The different OLED device structures based on Y5 are shown in Fig. 3a, and the corresponding EL parameters are summarized in Table 2 and Table S2 (Supporting information). The maximum EQE of OLEDs with the single-component ETLs are 0.45% (TPBi) and 0.41% (PDINN), respectively. The radiance and EQE change obviously when PDINN is mixed with TPBi. Gradually introducing TPBi into PDINN results in a trend of initially decreasing

Table 2
Optimized EL parameters of Y5-based OLEDs with the binary-mixed ETL or the single-component ones.

PDINN/TPBi	Emission Peak (nm)	EQE (%)	Radiance (W sr^{-1} m^{-2}) [a]	V_{on} (V)
1:0	887	0.41	30.0	1.27
1:4	892	0.50	34.9	1.24
0:1	897	0.45	32.5	1.20

[a] V_{on} was determined as the radiance reached 0.01 W sr^{-1} m^{-2}.

and then improving device performance. When TPBi is added to PDINN at a mixing ratio of 1:9 (10:90), the device performance decreases, showing inferiority compared to the single-component-ETL devices. We optimized the PDINN:TPBi ratio and found that the optimal ratio was 1:4 (20:80). As shown in Fig. 3b, OLED with binary-mixed ETL(PDINN:TPBi = 1:4) exhibits great increase in current density, which demonstrates that the electron injection efficiency is markedly improved compared with that of the reference devices. Moreover, the V_{on} decreases to 1.24 V, while the maximum EQE increases from 0.41% to 0.50% compared with devices with a single PDINN ETL (Fig. 3c). The reduction of the electron injection barrier is responsible for this phenomenon (*vide infra*). The results illuminate that the device with the ETL of PDINN:TPBi has better performance than that of the device with the ETLs of PDINN or TPBi. Fig. 3d shows the normalized EL spectra of OLEDs with different ETLs. Obviously, these devices exhibit NIR emissions with a peak near 900 nm. Devices with the binary-mixed ETL show a certain shift of emission peak compared to those with a single-component ETL. We notice that these devices show efficiency roll-off under high current density as shown in Fig. 3c. For fluorescent OLEDs, exciton−polaron interaction, carrier imbalance, and Joule heating are mainly responsible for the efficiency roll-off [40]. This effect may be ascribed to the electron-dominated characteristics of the non-fullerene small molecule fluorescent material Y5, which could result in a narrow exciton formation region and high exciton density leading to exciton quenching under high radiance or high current conditions.

In order to analyze the effect of the binary-mixed ETL on the electrical performance of the emissive layer, we prepared electron-only devices with the structures of ITO/ZnO/Y5/PDINN or PDINN:TPBi or TPBi/Ag (Fig. 4). The electron mobilities in devices with different ETLs obtained by SCLC method are summarized in Table S3 (Supporting Information). The obtained $J^{1/2}$–V curves are shown in Fig. 4a. The use of binary-mixed ETL sig-

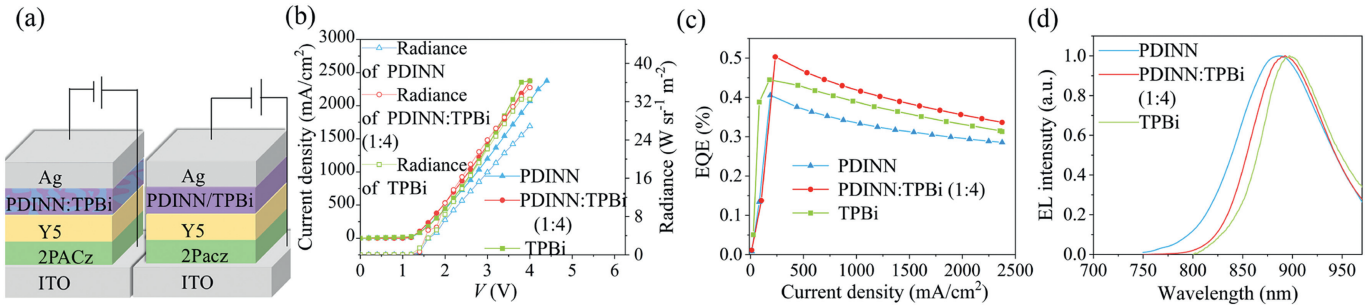

Fig. 3. Device structures (a), the current density–radiance–voltage (*J*–*R*–*V*) characteristics (b), EQE curves (c) and the EL spectra (d) of the NIR OLEDs with binary-mixed and the single-component ETL.

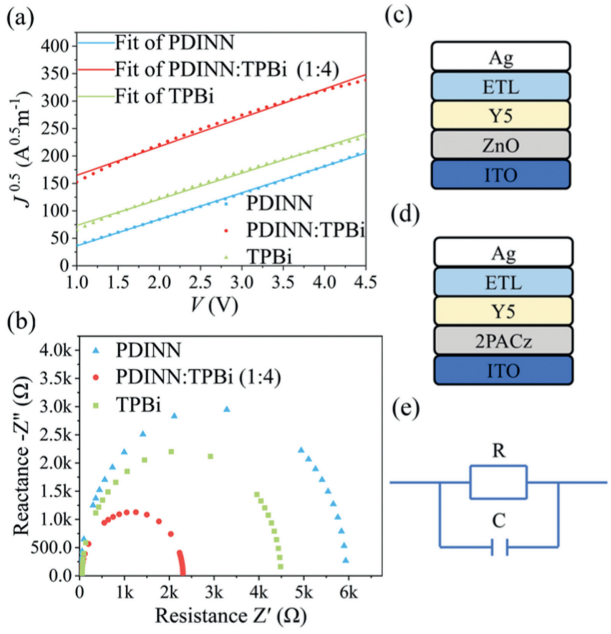

Fig. 4. (a) $J^{1/2}$–V curves and (b) the impedance spectra of devices with different ETLs in dark conditions. Device structures for (c) electron-only devices and (d) impedance test devices with different ETLs. (e) The equivalent circuit used for impedance spectrum analysis.

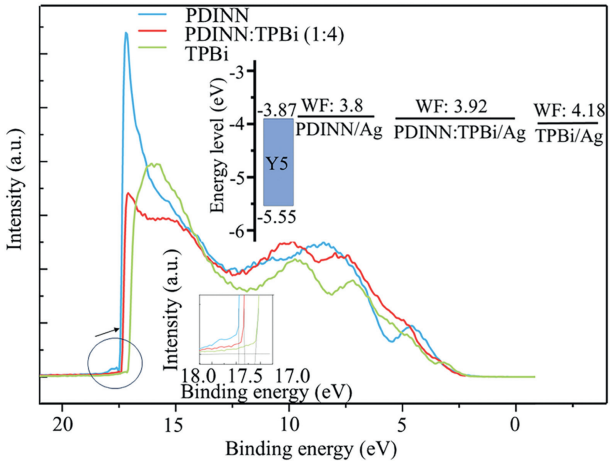

Fig. 5. UPS spectra of PDINN/Ag, PDINN:TPBi/Ag, and TPBi/Ag. Inset shows the energy-level alignments of the three ETLs relative to Y5.

nificantly increased the electron mobility from 7.64×10^{-4} cm^2 V^{-1} s^{-1} (PDINN) and 7.19×10^{-4} cm^2 V^{-1} s^{-1} (TPBi) to 9.22×10^{-4} cm^2 V^{-1} s^{-1} by up to ~20% at the optimal blend ratio, indicating that the binary-mixed ETL can significantly improve the electron transport.

To further understand the influence of the binary-mixed ETL on the charge injection and transport, AC impedance spectroscopy measurements were carried out and the results are shown in Fig. 4b. The device structure and equivalent circuit used for impedance analysis are shown in Figs. 4d and e. The corresponding resistance data are summarized in Table S4 (Supporting information). The impedance of OLEDs obviously decreases after introducing TPBi to PDINN, indicating decrease in the electron injection barrier and improvement of electron transport.

Exploring the mechanisms of driving voltage reduction and current efficiency improvement would be beneficial for understanding the interface engineering and promoting further optimization of OLEDs. Thus, we conducted ultraviolet photoelectron spectroscopy (UPS) to investigate the changes in work function (WF) of the cathodes combined with the three ETLs. The measured results are shown in Fig. 5, and the calculated WFs are shown in Table S5 (Supporting Information). For the PDINN/Ag sample, the secondary electron spectroscopy onset occurs with higher binding energy, leading to a lower WF of 3.80 eV by calculation, and for the TPBi/Ag sample, the secondary electron spectroscopy onset occurs with lower binding energy, leading to a higher WF of 4.18 eV. Upon blending the two components to form binary-mixed ETL (the PDINN:TPBi/Ag case), the corresponding WF changes to 3.92 eV. The observed WF changes suggest the successful formation of an alloy phase between PDINN and TPBi, which in turn influences the injection of electrons.

We also employed contact angle characterization to compare the surface properties of ETLs. As shown in Figs. 6a and b, the diiodomethane (DME) contact angle on the surface of PDINN:TPBi is 18°, which is smaller than that of PDINN (32°), while the contact angle of glycerol on the surface of PDINN:TPBi is 56°, which is greater than the contact angle of glycerol on PDINN (52°). Thus, the surface free energies (γ_s) of PDINN and PDINN:TPBi are calculated as 46.53 and 49.82 mN/m, respectively (Table S6 in Supporting information). The solubility parameter (δ) of PDINN is changed from 12.48 to 12.91 $(cal/cm^3)^{1/2}$ after introduction of TPBi. The Flory-Huggins interaction parameter (χ) between ETL and Y5 is changed from 0.40 (PDINN&Y5) to 0.53 (PDINN:TPBi&Y5) (Table S6). The bigger χ value indicates the interaction between molecules becomes weak (the repulsion arises), leading to poorer miscibility between the two components. The enlarged surface energy and interaction parameter can contribute to improvement in film formation and prevention of ETL penetration into EML, being beneficial to improve charge injection and reduces charge recombination, thereby improving the EQE [38,41]. It is worth mentioning that the χ between PDINN and TPBi is 0.38. A small χ also indicates that PDINN and TPBi can be blended well.

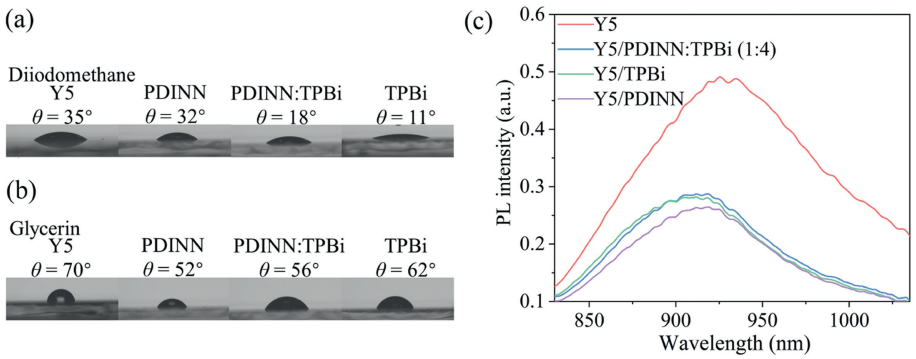

Fig. 6. Contact angles of (a) diiodomethane and (b) glycerol on Y5, PDINN, PDINN:TPBi, and TPBi films. (c) The PL spectra of Y5 and Y5/ETL films on quartz under 820 nm excitation.

We then tested the PL spectra of the EML Y5 in contact with/without three ETLs (Fig. 6c). As can be seen that less PL quenching is observed at the Y5/PDINN:TPBi or Y5/TPBi interface compared with Y5/PDINN interface. Based on the results of other research groups [36], we can attribute the effective exciton restraint function of TPBi and the improvement of carrier injection/balance at EML/ETL interfaces through self-balancing effect, which is beneficial to improving conductivity. The enhanced device performance of the binary-mixed ETL devices primarily stems from the synergistic effect of both transport materials, which collectively enhance charge transport in OLED devices. And the quenching of Y5 fluorescence in the EML by the electron transport layer is attenuated.

In summary, we synergistically integrated the merits of PDINN and TPBi for application as an ETL in NIR OLEDs, resulting in an enhanced carrier injection/transport performance in devices and weakened fluorescence quenching of the EML by simply blending TPBi with PDINN. Consequently, replacing the original single-component ETLs with a PDINN:TPBi binary-mixed ETL improves the EQE of NIR OLED when utilizing Y5 as the EML. Moreover, the full solution processing method and non-doped EML for this kind of NIR OLED will facilitate future industrial production.

Declaration of competing interest

The authors declare that they have no known competing financial interests or personal relationships that could have appeared to influence the work reported in this paper.

CRediT authorship contribution statement

Haowen Shang: Writing – original draft, Methodology, Investigation. **Yujie Yang:** Methodology, Formal analysis. **Bingjie Xue:** Visualization, Methodology. **Yikai Wang:** Methodology. **Zhiyi Su:** Methodology. **Wenlong Liu:** Methodology. **Youzhi Wu:** Writing – review & editing, Validation, Supervision. **Xinjun Xu:** Writing – review & editing, Supervision, Funding acquisition, Conceptualization.

Acknowledgments

This work was supported by the National Natural Science Foundation of China (No. 51973020) and Beijing Natural Science Foundation (No. 2232052). A portion of this work is based on the data obtained at BSRF-1W1A. The authors gratefully acknowledge the cooperation of the beamline scientists at BSRF-1W1A beamline.

Supplementary materials

Supplementary material associated with this article can be found, in the online version, at doi:10.1016/j.cclet.2024.110511.

References

[1] R.Q. Li, J. Wang, Y. Qin, et al., Org. Electron. 76 (2020) 105445.
[2] Y.H. Chen, S.Q. Chu, R.Q. Li, et al., Org. Electron. 66 (2019) 1–6.
[3] X.W. Zhang, M.K. Zhang, M.H. Liu, et al., Org. Electron. 53 (2018) 353–360.
[4] X. Zhang, J. Zhang, J. Wang, et al., Org. Electron. 58 (2018) 25–32.
[5] Y.H. Chen, L. Hao, X.W. Zhang, et al., J. Appl. Phys. 122 (2017) 065304.
[6] G. Qian, Z. Zhong, M. Luo, et al., Adv. Mater. 21 (2009) 111–116.
[7] X. Ai, E.W. Evans, S.Z. Dong, et al., Nature 563 (2018) 536–540.
[8] D.H. Kim, A. D'Aléo, X.K. Chen, et al., Nat. Photonics 12 (2018) 98–104.
[9] D.G. Congrave, B.H. Drummond, P.J. Conaghan, et al., J. Am. Chem. Soc. 141 (2019) 18390–18394.
[10] W.C. Chen, B. Huang, S.F. Ni, et al., Adv. Funct. Mater. 29 (2019) 1903112.
[11] O.T. Bruns, T.S. Bischof, D.K. Harris, et al., Nat. Biomed. Eng. 14 (2017) 0056.
[12] A. Minotto, I. Bulut, A.G. Rapidis, et al., Light Sci. Appl. 10 (2021) 18.
[13] J.Q. Wu, J. Appl. Phys. 106 (2009) 011101.
[14] A. Krier, D. Chubb, S. Krier, et al., Proc. IEEE Inst. Electr. Electron Eng. 145 (1998) 292–296.
[15] T. Someya, Z. Bao, G.G. Malliaras, Nature 540 (2016) 379–385.
[16] N. Tessler, V. Medvedev, M. Kazes, et al., Science 295 (2002) 1506–1508.
[17] J. Qi, W. Qiao, Z.Y. Wang, Chem. Rec. 16 (2016) 1531–1548.
[18] C.W. Tang, S.A. VanSlyke, Appl. Phys. Lett. 51 (1987) 913–915.
[19] L. Liao, K.P. Klubek, C.W. Tang, Appl. Phys. Lett. 84 (2004) 167–169.
[20] H. Uoyama, K. Goushi, K. Shizu, et al., Nature 492 (2012) 234–238.
[21] M.C. Gather, A. Köhnen, K. Meerholz, Adv. Mater. 23 (2011) 233–248.
[22] X.M. Wen, Y.G. Bi, F.S. Yi, et al., Opto-Electron. Adv. 4 (2021) 200024.
[23] S. Liu, W. Liu, J. Yu, et al., J. Mater. Chem. C 2 (2014) 835–840.
[24] Z.T. Li, K. Cao, J. Li, et al., Opto-Electron. Adv. 4 (2021) 200019.
[25] Y. Wang, S. Liu, F. Dang, et al., J. Phys. D: Appl. Phys. 45 (2012) 402002.
[26] X. Zhang, S. Liu, L. Zhang, et al., Adv. Opt. Mater. 7 (2019) 1800857.
[27] B. Li, Z. Yang, W. Gong, et al., Adv. Opt. Mater. 9 (2021) 2100180.
[28] K. Sun, D. Liu, W. Tian, et al., J. Mater. Chem. C 8 (2020) 11850–11859.
[29] H. Usta, D. Alimli, R. Ozdemir, et al., J. Mater. Chem. C 8 (2020) 8047–8060.
[30] M. Cai, T. Xiao, E. Hellerich, et al., Adv. Mater. 23 (2011) 3590–3596.
[31] J. Hwang, C. Lee, J.E. Jeong, et al., ACS Appl. Mater. 12 (2020) 8485–8494.
[32] N. Aizawa, Y.J. Pu, M. Watanabe, et al., Nat. Commun. 5 (2014) 5756.
[33] Y.J. Pu, T. Chiba, K. Ideta, et al., Adv. Mater. 27 (2014) 1327–1332.
[34] T. Chiba, Y.J. Pu, J. Kido, Adv. Mater. 27 (2015) 4681–4687.
[35] Y. Xie, W.S. Liu, W.Y. Deng, Nat. Photon. 16 (2022) 752–761.
[36] J. Yuan, Y. Zhang, L. Zhou, et al., Adv. Mater. 31 (2019) 1807577.
[37] Y.C. Wei, S.F. Wang, Y. Hu, et al., Nat. Photon. 14 (2020) 570–577.
[38] J. Yao, B. Qiu, Z.G. Zhang, et al., Nat. Commun. 11 (2020) 2726.
[39] S.M. Liu, B. Li, L. Zhang, S. Yue, Appl. Phys. Lett. 98 (2011) 163301.
[40] C. Murawski, K. Leo, M.C. Gather, Adv. Mater. 25 (2013) 6801–6827.
[41] J.Q. Wang, Z. Zheng, D.Y. Zhang, et al., Adv. Mater. 31 (2019) 1806921.